UCRL-JC-130520
PREPRINT

# In-Situ Spatially Resolved X-Ray Diffraction Mapping of the Alpha to Beta to Alpha Transformation in Commercially Pure Titanium Arc Welds

John W. Elmer
Joe Wong
Thorsten Ressler

This paper was prepared for submittal to the
5th International Conference on Trends in Welding Research
Pine Mountain, GA
June 1-5, 1998

May 15, 1998

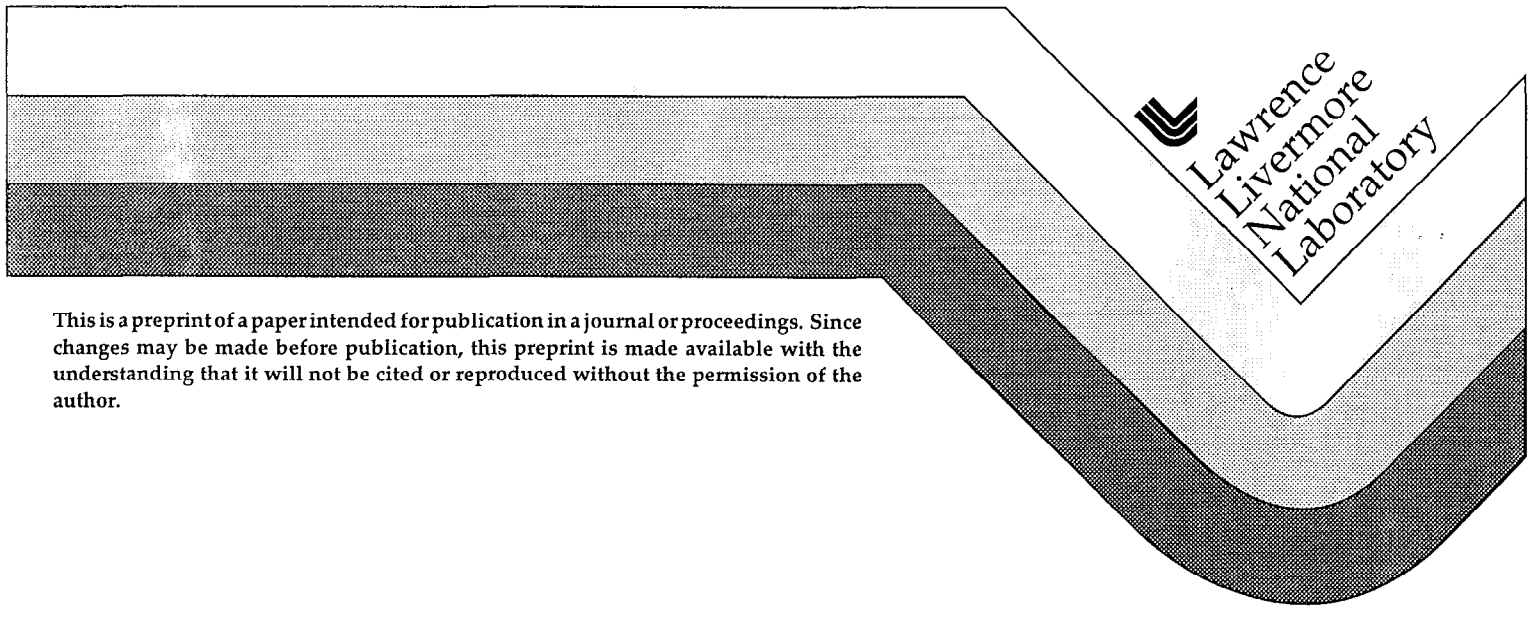

# In-Situ Spatially Resolved X-Ray Diffraction Mapping of the $\alpha \rightarrow \beta \rightarrow \alpha$ Transformation in Commercially Pure Titanium Arc Welds

*by*
*John W. Elmer, Joe Wong, and Thorsten Ressler*

*Lawrence Livermore National Laboratory*
*University of California, P. O. Box 808, Livermore, CA, 94551*

## Abstract

Spatially Resolved X-Ray Diffraction (SRXRD) is used to map the $\alpha \rightarrow \beta \rightarrow \alpha$ phase transformation in the heat affected zone (HAZ) of commercially pure titanium gas tungsten arc welds. *In-situ* SRXRD experiments were conducted on arc welds using a 200 μm diameter x-ray beam at Stanford Synchrotron Radiation Laboratory (SSRL). A map was created which identifies six HAZ microstructural regions that exist between the liquid weld pool and the base metal during welding. The first region is single phase β-Ti that forms in a 2- to 3-mm band adjacent to the liquid weld pool. The second region is back transformed α-Ti that forms behind the portion of the HAZ where β-Ti was once present at higher temperatures. The third region is completely recrystallized α-Ti that forms in a 2- to 3-mm band surrounding the single phase β-Ti region. Recrystallized α-Ti was observed by itself and also with varying amounts of β-Ti. The fourth region of the weld is the partially transformed zone where α-Ti and β-Ti coexist during welding. The fifth region is directly behind the partially transformed zone and consists of a mixture of recrystallized and back transformed α-Ti The sixth region is farthest from the weld pool and consists of α-Ti that is undergoing annealing and recrystallization. Annealing of the base metal was observed to some degree in all of the SRXRD patterns, showing that annealing exceeded 13 mm from the centerline of the weld. Although the microstructure consisted predominantly of α-Ti, both prior to the weld and after the weld, the (002) texture of the starting material was altered during welding to produce a predominantly (101) texture within the resulting HAZ.

## Introduction

This investigation studied commercially pure titanium welds that exhibit annealing and recrystallization in the colder portions of the HAZ, and both partial and complete $\alpha \rightarrow \beta$ transformation in the hotter portions of the HAZ [1]. In the completely transformed region of this material, the temperature/time history of the titanium is such that α-Ti transforms to single phase β-Ti during the weld heating cycle. During welding, the completely β-transformed region of the HAZ contains large grains due to the absence of α-Ti in this region of the weld to inhibit grain growth [1,2]. In the partially transformed region, the peak temperatures are above the α/β transition temperature, but the time above this temperature is insufficient to permit complete transformation of the low temperature α-Ti phase to the high temperature β-Ti phase. Hence, the microstructure in the partially transformed region of the HAZ during the weld heating cycle consists of a mixture of α-Ti plus β-Ti just prior to beginning the $\beta \rightarrow \alpha$ back transformation as the weld cools.

Although it is known qualitatively that these different regions exist around welds [3,4], the exact size and location of these zones has not been directly measured. One way to estimate the size of the HAZ regions is to calculate them from the heating cycle of the weld and the kinetic parameters of the phase transformations. However, kinetic parameters are rarely known for materials under actual welding conditions. These data are rare since the non-isothermal and transient heating occurring during welding induces complex HAZ phase transformation kinetics that are difficult to measure experimentally and model theoretically

SRXRD is being developed as a new experimental method for mapping the phases that exist in the HAZ in-situ during welding. Regions of annealing, recrystallization, partial $\alpha \rightarrow \beta$ transformation and complete $\alpha \rightarrow \beta$ transformation were identified in titanium. From this resulting phase map, the kinetics of phase transformations that occur under the highly non-isothermal heating and cooling cycles produced during welding can be better understood.

## Materials and Experimental Procedures

**Titanium Samples.** Grade 2 commercially pure titanium was purchased in 11.4 cm diameter bar stock. Chemical analysis was performed on this material using combustion analysis for O, C, N, and H, and inductively coupled plasma analysis for the

remaining elements. The results yield the following concentration (by wt.%) of impurities: 0.14% Fe, 0.17% O, 0.03% Al, 0.02% Cr, 0.008% C, 0.001% H, 0.014% N, 0.02% Ni, 0.005% V, 0.004% Si. Cylindrical welding samples were machined from the as received material into 10.2 cm diameter bars measuring 12.7 cm long. These samples had a surface finish of 1.6 μm rms and were round to within 10 μm on the diameter.

**Welding.** Gas tungsten arc welds were made on the titanium bars using a 150 A direct constant current welding power supply with electrode negative polarity. The welding electrode was made of W-2% Th and measured 4.7 mm diameter. A new electrode was used for each weld and was straight ground with a 90° included angle taper. The power was maintained constant at 1.9 kW (100 A, 19 ± .5 V) for all of the welds, and helium was used as the welding and shielding gas. The titanium bar was rotated at a constant speed of 0.20 rpm below the fixed electrode, which corresponded to a surface welding speed of 1.1 mm/s, and resulted in an 11 to 12 mm wide fusion zone on the surface of the titanium bar.

All welding was done inside an environmentally controlled chamber to minimize oxidation of the titanium during welding [5]. Prior to welding, the vacuum chamber was evacuated to 60 mTorr using a mechanical roughing pump and then back-filled with high purity (99.999%) helium gas. Post weld inspection showed the fusion zone to have a bright silver appearance and the HAZ to have a light silver-gray appearance.

The welding assembly was integrally mounted to a translation stage driven by a stepper motor with 10 μm precision and placed inside the environmental chamber. Spatial mapping of the phases in the HAZ was performed using the translation stage to manipulate the weld (welding torch and workpiece) with respect to the fixed x-ray beam in order to probe discrete regions around the weld. Movements perpendicular to the centerline of the weld were controlled by a computer and were performed by direct translation of the workpiece with respect to the x-ray probe. An in-house designed software package was developed on a personal computer using LabView software version 4.0 to control the position of the weld with respect to the x-ray beam, and the bar rotational speed (welding speed), and to trigger the data acquisition system on a second computer.

**Spatially Resolved X-Ray Diffraction.** SRXRD measurements were performed on the 31-pole wiggler beam line, BL 10-2 [6] at SSRL with the SPEAR (Stanford Positron-Electron Accumulation Ring) operating at an electron energy of 3.0 GeV and an injection current of ~100 mA. Details of the SRXRD welding experiments have been previously published [1] so only a brief description will be given later to highlight some modifications to the technique.

SRXRD data was taken during welding by positioning the beam at a fixed location with respect to the welding electrode and collecting data for 6 s while the bar rotated under the torch at a constant speed. Data points were taken during one revolution of the weld around the cylinder by incrementally jogging the weld in 200 μm steps to new probe locations at 6 s intervals. In this way a series of x-ray diffraction patterns was collected for a given weld along a scan direction perpendicular to and away from its centerline. After completing a run, the weld was allowed to cool to room temperature and was then repositioned to a new starting location with respect to the x-ray beam prior to taking the next series of data.

The SRXRD experiments were performed using a focused monochromatic synchrotron x-ray beam. The synchrotron white beam emerging from the 31-pole wiggler was first focused by a toroidal mirror to the source size of ~1 × 2 mm, and then monochromatized with a double Si (111) crystal. The focused monochromatic beam was then passed through a 180 μm tungsten pinhole to render a 200 μm beam on the sample at an incident angle of ~25°. This setup yielded a beam flux on the sample of $\sim 10^{10}$ photons/s determined experimentally using an ion chamber downstream from the pinhole. A photon energy of 8.5 keV ($\lambda = 0.14586$ nm) was chosen as an optimum energy to: (a) maximize the penetration depth in Ti (~26 μm); (b) minimize the background contribution due to Ti K-fluorescence from the sample (Ti K-edge at 4966 eV [7]); (c) stay within the specified detection efficiency range (<10 keV) of the silicon photodiodes; and (d) maximize the range of 2θ to collect an adequate number of diffraction peaks for both the hcp and bcc phases of Ti for phase identification.

SRXRD diffraction patterns were recorded behind the weld using a 50-cm long 2048 element position sensitive Si photodiode array detector. The array was mounted on a dual-stage Peltier effect thermoelectric cooler, which in turn was water cooled. This detector was placed ~10 cm behind the weld to cover a 2θ range from 30° to 60° This range of 2θ was optimized for phase identification to contain five of the major α-Ti diffraction peaks and two for the β-Ti. The detector and associated ST121 data acquisition system was manufactured by Princeton Instruments and was used to store and display the x-ray diffraction data in real time.

**Materials Characterization.** Optical metallography was performed on as-received titanium and on-post welded samples using conventional polishing and etching techniques. Etching was performed in a chemical bath of 15 parts lactic acid, 5 parts nitric acid and 1 part hydofluoric acid. Photographs of the as polished microstructures were taken under polarized light conditions.

**The α→β Transformation Temperature.** Two different phase transitions occur in pure titanium: the α→β phase transformation in the solid state at 882°C and melting at 1668°C [8]. In Grade 2 titanium these same two transitions occur, but the α→β transition temperature is altered by the presence of iron, oxygen, and other impurities [8]. The transformation temperature, or range of temperatures, for Grade 2 titanium was investigated using the Gleeble. These tests were conducted by rapidly heating the sample to a given temperature, isothermally holding at this temperature for 15 minutes to allow the microstructure to stabilize, and rapidly cooling the sample back to room temperature.

The results showed partial α→β transformation up to 910°C, and complete transformation for samples held at 920°C or

higher. From these microstructural observations it was concluded that in Grade 2 titanium the α-Ti phase begins to transform to β-Ti at temperatures between 880°C and 890°C, and that this transformation is not complete until temperatures reach between 910°C and 920°C. This is within the reported temperature range of the β-Ti transus of 913°C ± 15°C for commercially pure titanium having an oxygen content of 0.25 wt.% maximum [9]. For the purpose of this investigation, it was concluded that this commercially pure titanium can be treated as a titanium alloy with an α/(α+β) equilibrium temperature of 885 ± 5°C and an β/(β+α) equilibrium transus temperature of 915 ± 5°C.

## Results

**Post-Weld Microstructures.** The microstructure of the HAZ was revealed by lightly polishing and etching the surface of the welded titanium bar in the same locations relative to the fusion zone where the SRXRD data was obtained. Figure 1 shows the HAZ microstructures, indicating that a gradient in microstructures that develops as the time/temperature kinetic strength of the HAZ increases from the base metal toward the liquid weld pool.

The base metal microstructure is shown in Fig. 1(a) and is composed of heavily twinned and elongated α-Ti grains with a dark etching minor constituent phase that is elongated along the extrusion direction of the bar. The dark particles were characterized to exhibit both bcc and omega crystal structure using selected area diffraction in the TEM [10].

The annealed and partially recrystallized region of the HAZ is shown in Fig. 1(b) at a distance of ~5 mm from the fusion line. This microstructure has recrystallized to produce fine equiaxed α-Ti grains (~20 μm diameter) that are less twinned than those of the base metal. The dark secondary phase is still present in the microstructure in the same proportions as that of the base metal.

The fully transformed region of the HAZ is shown in Fig. 1(c) at a distance of ~0.4 mm from the fusion line. This microstructure is composed of large equiaxed prior β-Ti grains (250 μm diameter) that transformed back to α-Ti as the weld cooled. The secondary phase is now distributed within the microstructure and still retains both bcc and omega diffraction patterns in the TEM.

**SRXRD Diffraction Patterns.** SRXRD experiments were performed during welding to determine which phases, either α-Ti or β-Ti, were present at various locations within the HAZ. These experiments were performed during welding by observing the diffraction patterns of these two phases.

Representative SRXRD patterns taken from the weld HAZ [10,11] are compared with those of the base metal in Fig. 2. These diffraction patterns show the effects of annealing, recrystallization, grain growth of the recrystallized grains, and the back transformation of β-Ti to α-Ti behind the weld. In this figure, (α) represents the base metal (hcp) α-Ti phase. ($\alpha_{AR}$) is

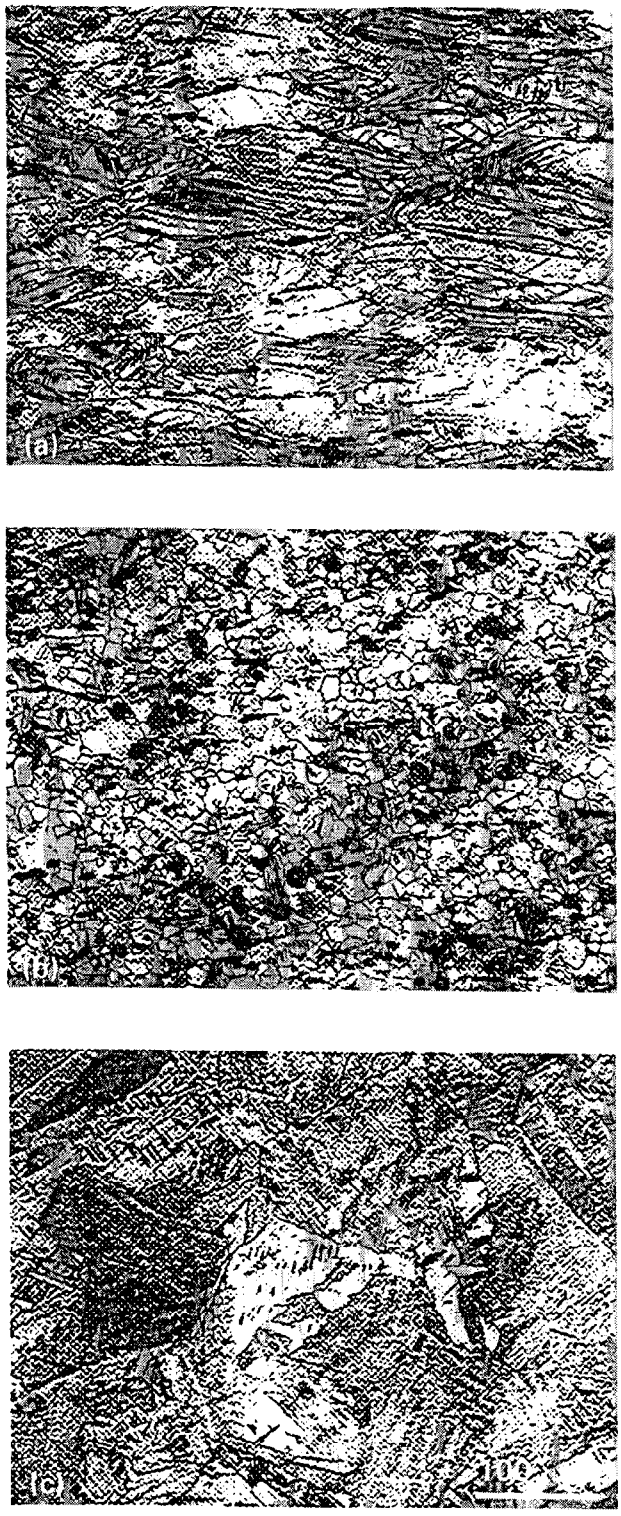


Fig. 1. Optical micrographs of the base metal and HAZ microstructures. (a) Base metal prior to welding; (b) Annealed and partially recrystallized HAZ region, ~5 mm from the fusion line; (c) Fully transformed HAZ region, ~0.4 mm from the fusion line. All micrographs were taken at the same magnification.

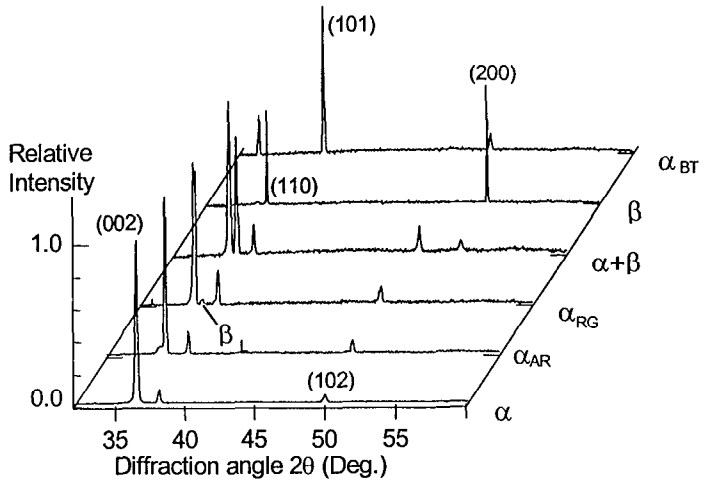


Fig. 2. Typical diffraction patterns from titanium welds. These diffraction patterns represent the different regions that exist in the HAZ during welding.

the annealed and/or recrystallized α-Ti. ($\alpha_{RG}$) denotes recrystallized α-Ti phase undergoing grain growth and exhibiting large diffraction domains. ($\alpha_{BT}$) is the back transformed α-Ti formed from the region of the HAZ that once contained β-Ti. (β) is single-phase β-Ti, and ($\beta_L$) is the β-Ti that coexists with α-Ti in low amounts predominantly together with $\alpha_{BT}$. Data were normalized to unity for the highest peak in each pattern. A detailed crystallographic analysis of these patterns is presented in a separate article [11].

Figure 3 shows x-ray diffraction patterns from one of the SRXRD runs. In this run the beam was initially positioned in the HAZ at a location starting at X=−6 mm, ahead of the weld, and Y=1 (see Fig. 4 for coordinates). Initially, the beam was located in the β-Ti region, but as it moved farther away

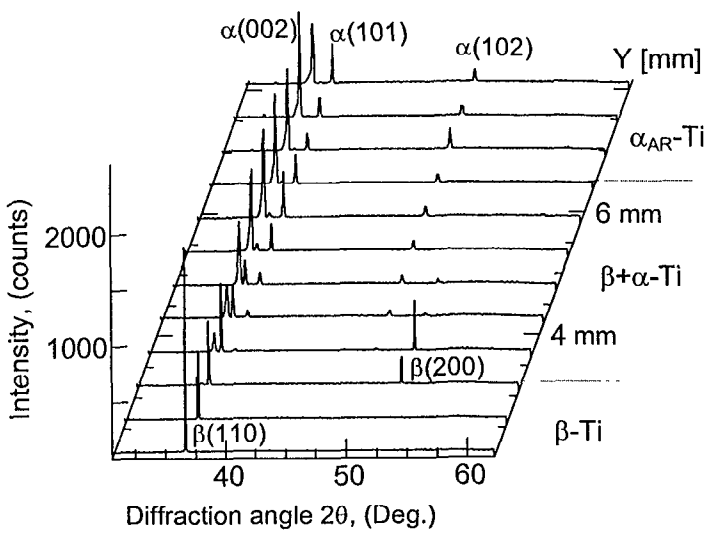


Fig. 3. Evolution of SRXRD patterns measured across the α→β phase transformation isotherm. The α- and β-Ti region as well as β+α coexistence zone are shown.

from the weld centerline it passed through the α+β-Ti region and then the α-Ti region of the HAZ. These different zones are identified through changes in the x-ray diffraction patterns.

## Discussion

**SRXRD Diffraction Map of the HAZ.** Sequential linear x-ray scans such as those presented in Fig. 3. were combined to create a map of the diffraction patterns, and thus the phases, which exist in the HAZ during welding. This map is shown in Fig. 4, where the stationary welding electrode is positioned at X=Y=0, with metal moving beneath the welding torch from left to right along the X-axis. The SRXRD results are plotted such that two sets of diffraction data are presented side-by-side when both α-Ti and β-Ti were present in the same run. The left side of each data set represents the locations where SRXRD showed the presence of α-Ti, and the right side of each data set represents the locations where SRXRD showed the presence of β-Ti. Many of these data sets overlap for some distance. These overlapped regions along the Y-axis indicate the zone where both phases coexisted during welding.

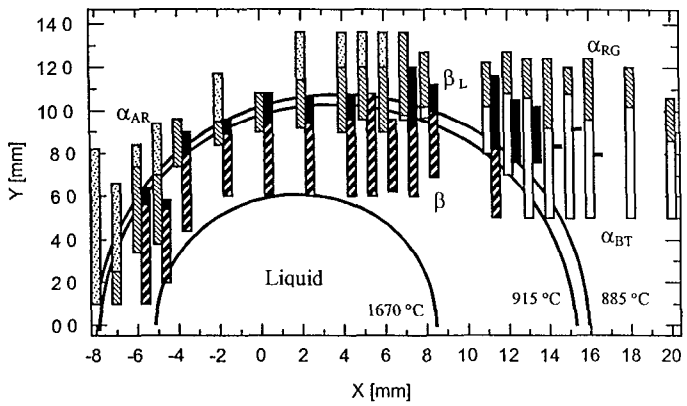


Fig. 4. SRXRD map showing the locations of all of the Ti diffraction patterns with respect to the calculated isotherms for a titanium weld.

In addition to defining the individual phases, each data set in Fig. 4 is further subdivided into regions with different shadings to indicate the different types of observed diffraction patterns that were present at these locations. $\alpha_{AR}$ is shown with small dots; $\alpha_{RG}$ is shown with right diagonal stripes; $\alpha_{BT}$ is solid white; β is shown with left diagonal stripes; and $\beta_L$ is solid black.

Superimposed on this plot are three weld isothermal boundaries that were calculated using an analytical heat flow model for welds [10], and a mirror symmetry about the weld centerline is assumed. The calculated liquidus isotherm at 1670°C represents the liquid weld pool boundary and has a maximum width of 12 mm. The α/(α+β) isotherm at 885°C is plotted to represent the location where α can first begin to transform to β on heating and where β would complete transforming to α on cooling [10] under equilibrium conditions.

The β/(β+α) transus isotherm at 915°C is plotted to represent the location where α would complete transforming to β on heating and where β can first begin to transform to α on cooling [10] under equilibrium conditions.

This map shows the spatial relationship among the regions of α-Ti annealing and recrystallization, α→β transformation, and β→α transformation. Since the metal is moving at a constant speed of 1.1 mm/s beneath the stationary arc, the spatial coordinates presented in this map can be converted to the heating or cooling duration, by dividing the distance over which the transformation takes place and the speed of the weld.

**Annealing.** Annealing of the initially worked α-Ti base metal was observed to distances greater than 13.0 mm from the centerline of the weld. The distance that the metal is annealed represents the true extent of the HAZ, however, the range of SRXRD data obtained in this investigation was not large enough to encompass the entire annealed region. Therefore, the base metal/$\alpha_{AR}$ boundary was not determined.

Figure 5 highlights the annealed and recrystallized HAZ region ($\alpha_{AR}$) of the HAZ as determined by SRXRD. The diffraction patterns show a gradual transition from the base metal pattern to one of narrower peaks that exhibit low 2θ shoulders as the material anneals and recrystallizes [10,11]. The $\alpha_{AR}$ pattern occurs principally on the leading edge of the HAZ where the weld is heating.

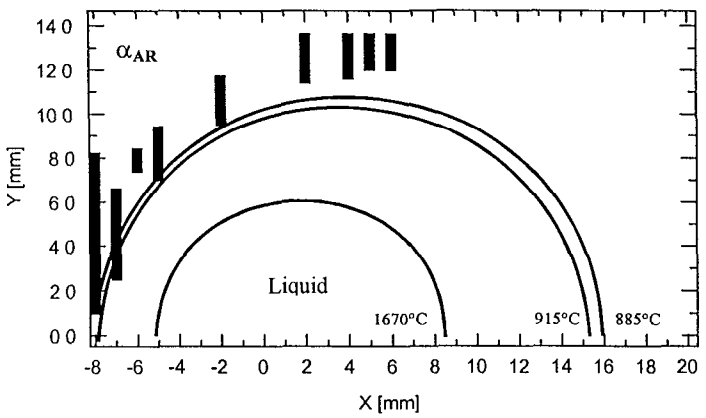


Fig. 5. Locations where the $\alpha_{AR}$ diffraction pattern was observed by SRXRD. This region consists of annealed and partially recrystallized α-Ti grains.

**Recrystallization.** The α-Ti grains initially began to recrystallize in the $\alpha_{AR}$ region but continued the process into the $\alpha_{RG}$ region. As the recrystallized grains remain at elevated temperatures, they grow until the temperature drops as the grains pass farther behind the weld. The growth of the recrystallized grains was detected by changes in the diffraction patterns [10,11].

Figure 6 highlights the $\alpha_{RG}$ region that extends in a curved path that follows the shape of the weld isotherms on the front side of the weld then trails behind the weld. The $\alpha_{RG}$ region can exist by itself or it can coexist with β-Ti in the mixed α+β region of the HAZ. Growth of the recrystallized grains was observed as far out as 13 mm from the centerline, and these effects remained after the weld had cooled.

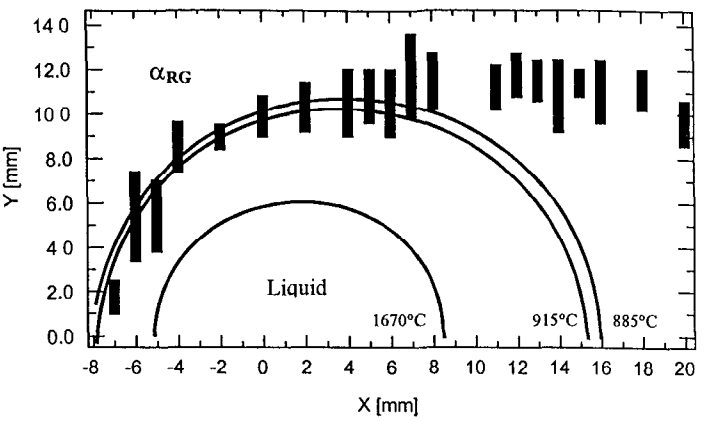


Fig. 6. Locations where the $\alpha_{RG}$ diffraction pattern was observed. This region consists of recrystallized α-Ti grains that are undergoing grain growth.

**The α→β Transformation.** During the α→β transformation, both α-Ti and β-Ti coexist for some time. The initial stages of the transformation appear in the diffraction patterns as a small bcc(110) peak, $\beta_L$, growing between the hcp (002) and hcp(101) peaks as indicated in Fig. 2. This $\beta_L$ region is highlighted in Fig. 7, which was observed on both the leading (heating) and trailing (cooling) sides of the weld. The integrated intensity ratio of the $\beta_L$ peak to that of the α-Ti is estimated to be less than 0.1 [11].

During heating, the $\beta_L$ peak grows as the material moves into hotter portions of the HAZ as shown in Fig. 3. The region where both α-Ti and β-Ti coexist on the leading side of the weld represents the region where α-Ti is transforming to β-Ti. This partially transformed region occurs at distances between 9.0 and 10.7 mm from the centerline of the weld, see Fig. 4.

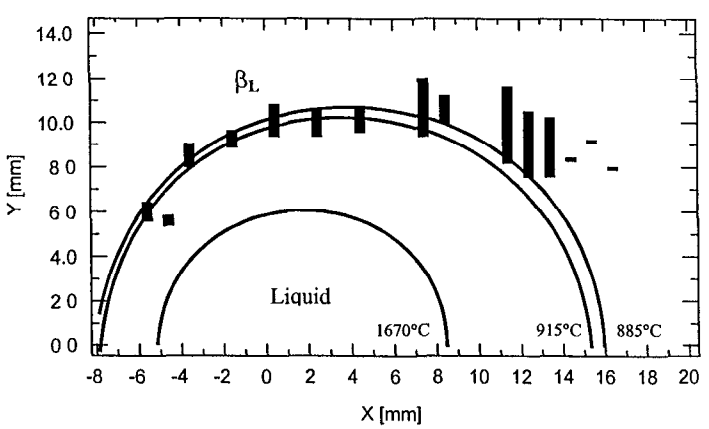


Fig. 7. Locations where the $\beta_L$ diffraction pattern was observed. This region represents both the initial stage of the α→β and the final stage of the β→α transformations.

**The Complete Transformation to β-Ti.** For locations close enough to the centerline of the weld, the α-Ti will completely

transform to β-Ti. The region where β-Ti was observed by SRXRD is highlighted in Fig. 8. This broad region surrounds the liquid weld pool and extends out to the α+β two phase region. Single phase β-Ti was observed at distances as far as 9.0 mm from the centerline of the weld, and this region falls within the calculated β/(β+α) isotherm. Grain growth of the β-Ti grains is rapid in this part of the HAZ due to the absence of α-Ti to impede grain growth.

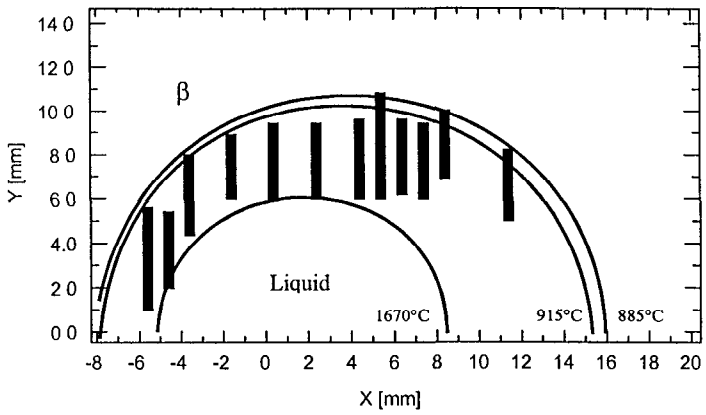


Fig. 8. Locations where the β diffraction pattern was observed. This region represents the portion of the HAZ where the α→β transformation is complete.

**The β→α Transformation.** On the trailing side of the weld, the portions of the HAZ that had transformed partially or completely to β-Ti begin to transform back to α-Ti. The back transformed α-Ti phase is identifiable from a diffraction standpoint because the crystallographic texture changes from predominantly hcp (002) texture before the weld to a predominantly hcp (101) texture after the weld as indicated in Fig. 2.

Figure 9 highlights the back transformed $\alpha_{BT}$ region of the weld. This back transformed titanium was observed from the fusion line to distances as far as 10.7 mm from the centerline of the weld and continued to be present after the weld had cooled.

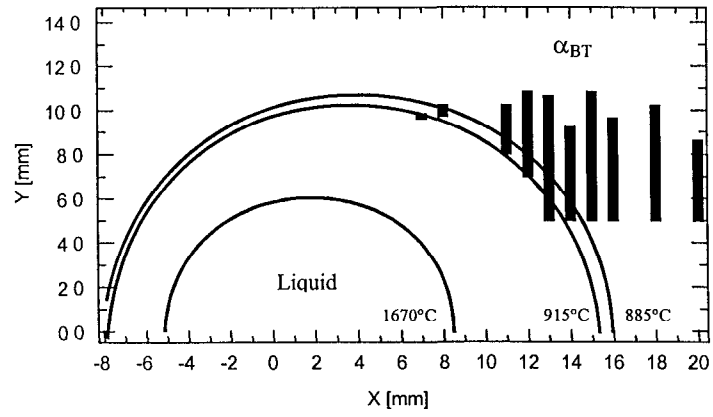


Fig. 9. Locations where the $\alpha_{BT}$ diffraction pattern was observed. This represents the region of the HAZ after the β→α transformation is complete.

## Conclusions

1. *In-situ* spatially resolved x-ray diffraction was used to map the α→β→α phase transformation in the HAZ of commercially pure titanium gas tungsten arc welds.
2. The effects of annealing, recrystallization, and α→β phase transformation contribute to six microstructural HAZ regions around the liquid weld pool: single phase β-Ti; back transformed α-Ti; fully recrystallized α-Ti; α–Ti plus β-Ti coexistence; recrystallized α-Ti and back transformed α-Ti coexistence; and α-Ti undergoing annealing/recrystallization.
3. Changes in crystallographic texture occurred in the locations of the HAZ that had undergone the α→β→α transformation. The change in texture was from the predominantly (002) α-Ti orientation before the weld to the predominantly (101) α-Ti orientation after the weld.

## Acknowledgments

This work was performed under the auspices of the U. S. Department of Energy, Lawrence Livermore National Laboratory, under Contract No. W-7405-ENG-48. This work was supported by DOE, Office of Basic Energy Sciences, Division of Materials Science. Synchrotron experiments were conducted at SSRL supported by DOE, Division of Chemical Science. T. Ressler wishes to thank the Alexander von Humboldt Foundation for a Feodor Lynen research fellowship. The authors express gratitude to W. Lin of EWI for the Gleeble testing, A. T. Teruya of LLNL for writing LabView software, and B. Kershaw of LLNL for optical metallography.

## References

1. J. W. Elmer, Joe Wong, M. Fröba, P. A Waide, and E M Larson: *Metall. Mater. Trans A*, 1996, 27A(3), p. 775
2. T. R. McNelly and H. Charles Heikkenen: Superplasticity in Aerospace II, edited by T R McNelly and H Charles Heikkenen, from the *119th meeting of TMS*, pp. 317-332, 1990
3. Ø. Grong: Metallurgical Modelling of Welding, *The Institute of Materials*, London, Chapter 1, 1994.
4. K. Easterling: Introduction to the Physical Metallurgy of Welds, *Butterworths and Co.*, Chapter 3, 1983
5. Joe Wong, M. Fröba, J W Elmer, P. A Waide, and E M Larson: In Situ Phase Mapping and Transformation Study in Fusion Welds, *J Mater. Sci.*, 1997, 32, pp 1493.
6. V. Karpenko, J.H. Kinney, S Kulkarni, K Neufeld, C Poppe, K.G. Tirsell, Joe Wong, J Cerino, T. Troxel, J. Yang, E. Hoyer, M. Green, D Humpries, S. Marks, and D. Plate: *Rev Sci Instrum*, 1989, 60, pp 1451-1460
7. A. Bearden and A. F. Burr: *Rev. Mod Phys*, 1967, vol. 39, pp 125-37.
8. C W. Dawson and S. L Sass: *Metallurgical Transactions*, 1970, v1, pp. 2225-2233.
9. Binary Alloy Phase Diagrams, *ASM International*, second edition, 1990.
10. J. W. Elmer, Joe Wong, and T. Ressler: submitted to *Metall and Mater. Trans A*, April, 1998, LLNL UCRL-JC-130061, 1998
11. T. Ressler, Joe Wong, and J. W. Elmer: will submit to *J Phys, Chem*, May, 1998.

*Technical Information Department* • **Lawrence Livermore National Laboratory**
**University of California • Livermore, California 94551**